optica

Infrared frequency comb generation and spectroscopy with suspended silicon nanophotonic waveguides: supplementary material

Nima Nader[1,*], Abijith Kowligy[2,+], Jeff Chiles[1,+], Eric J. Stanton[1], Henry Timmers[2], Alexander J. Lind[2,3], Flavio C. Cruz[2,4], Daniel M. B. Lesko[2,3], Kimberly A. Briggman[1], Sae Woo Nam[1], Scott A. Diddams[2,3,*], and Richard P. Mirin[1,*]

[1] Applied Physics Division, National Institute of Standards and Technology, 325 Broadway, Boulder, Colorado 80305, USA
[2] Time and Frequency Division, National Institute of Standards and Technology, 325 Broadway, Boulder, Colorado 80305, USA
[3] Department of Physics University of Colorado, 2000 Colorado Avenue, Boulder, Colorado 80309, USA
[4] Instituto de Fisica Gleb Wataghin, Universidade Estadual de Campinas, Campinas, SP, 13083-859, Brazil
[*] Corresponding authors: nima.nader@nist.gov, scott.diddams@nist.gov, richard.mirin@nist.gov
[+] These authors have contributed equally to this work.

This document provides supplementary information to "Infrared frequency comb generation and spectroscopy with suspended silicon nanophotonic waveguides," https://doi.org/10.1364/optica.6.001269. This document contains four sections. Section 1 explains the details of the suspended Si waveguides fabrication. Section 2 gives a detailed explanation of the generalized nonlinear Schrödinger equation used to model the generated supercontinuum spectra at different waveguide widths. Section 3 explains the baseline fitting and subtraction to study dual-comb measured atmospheric water absorbance data. We also explain the detailed procedure for the comparison of the data with HITRAN database to estimate the experimental atmospheric pressure and water content. Section 4 provides the detailed process for background subtraction of the broadband liquid-phase dual-comb data. Section 5 goes through the detailed spectral peak assignments of the measured vibrational lines in DCS of isopropanol and methanol.

1. WAVEGUIDE FABRICATION

We fabricate suspended-Si waveguides following the method presented in [1]. The process starts with two wafers (Fig. S1a), namely one prime-grade Si and a Si-on-Insulator (SOI). The SOI wafer has a 700 nm thick Si device layer on top and a 500 nm thick buried oxide underneath (Fig. S1a). Both wafers are solvent- and H_2SO_4:H_2O_2-cleaned prior to the processing. Suspended waveguide trenches are patterned in a positive tone photoresist by 405 nm lithography. These patterns are transferred to the prime-Si wafer with an etch depth of 15 μm by reactive ion etching (RIE) with SF_6:C_4F_8 based chemistry (Fig. S1b).

After this step, both wafers are prepared for wafer bonding as follows: The native oxide on both wafers is removed with a diluted, 5%, buffered-oxide-etch (BOE), making both surfaces hydrophobic. Wafers are then transferred to an atmospheric plasma system for surface activation in a N_2:H_2 plasma. When completed, this plasma activation makes the bonding interfaces hydrophilic. Wafers are then soaked in water to saturate the activated surfaces with –OH groups. After drying, wafers are placed in contact in an atmospheric wafer bonder to initiate the temporary bond (Fig. S1c), assisted by Van der Waals forces between the hydroxyl groups. To make the bond permanent, the wafer stack is annealed at 300 C for 6 hours in a N_2-purged
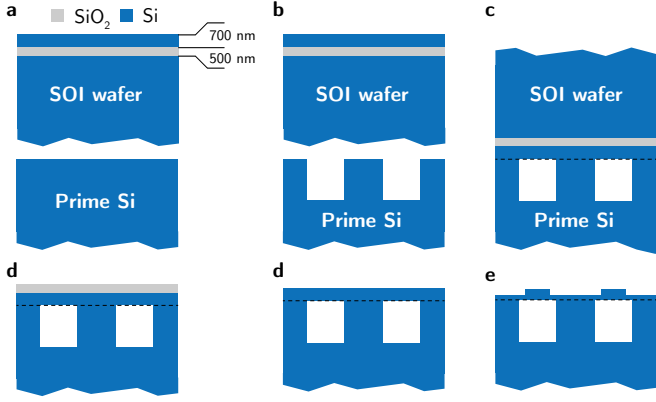
Fig. S1. Schematic diagram of the suspended-Si waveguide fabrication steps. (a) The prime-Si and the Si-on-insulator wafers used in the process. (b) RIE etching of the suspended waveguide trenches in the prime-Si wafer. (c) Wafer bonding. (d) Backside Si wafer removal with (e) BOE removal of the buried oxide layer. (f) Patterning and etching of the waveguide structures.

furnace. The annealing process replaces the OH–OH bonds with Si–O–Si fusion bonds and the released gases exit the bond interface through the suspended waveguide trenches. During this step, trenches act as gas release channels to minimize bond voids, and therefore increasing the fabrication yield significantly. We continue the processing by removing the backside Si wafer (Fig. S1d) and the buried oxide layer (Fig. S1e) with RIE etching and diluted BOE, respectively.

A 200 nm thick SiO_2 hard mask is deposited on the Si membrane prior to patterning and etching of the waveguides. A positive tone electron-beam (e-beam) lithography resist is spin-coated with the thickness of ~ 400 nm on the hard mask and waveguide structures are patterned using an e-beam writer. The patterns are RIE etched in the SiO_2 hard mask using a CHF_3 chemistry. Following the hard mask etch, e-beam resist is solvent-removed and the waveguide structures are transferred to the suspended-Si membrane using a HBr-chemistry RIE etch (Fig. S1f). The waveguide patterning ends with hard mask removal with 5% BOE. The same step is repeated to pattern and etch the floating fork-shaped couplers but with minor differences. Namely, a thicker hard mask (~ 300 nm) and a thicker e-beam resist (~ 780 nm) are used to support the full etch of the 700 nm thick Si membrane to achieve floating structures. The fabrication process ends with a die release step using a chemical dicing recipe based on deep-RIE etching of Si.

2. SUPERCONTINUUM GENERATION MODELING

We use the generalized nonlinear Schrödinger equation (gNLSE) [2] to model supercontinuum generation in the suspended-Si waveguides. The equation is written as [3]:

$$\frac{\partial E(z,t)}{\partial z} - i \sum_{k \geq 2} i^k \frac{\beta_k}{k!} \frac{\partial^k E}{\partial \tau^k} E(z,t) =$$

$$-\frac{\alpha}{2} E(z,t) + (1 + \frac{i}{\omega_0}\frac{\partial}{\partial \tau})(i\gamma|E|^2 E - \frac{\beta_{3PA}}{3A_{eff}^2}|E|^4 E) - \frac{\sigma}{2}(1 + i\mu)N_c E$$

(S1)

where z is the propagation direction, β_k is the k$^{\text{th}}$-order dispersion of the waveguide, $\tau = t - \beta_1 z$ is the temporal-coordinate
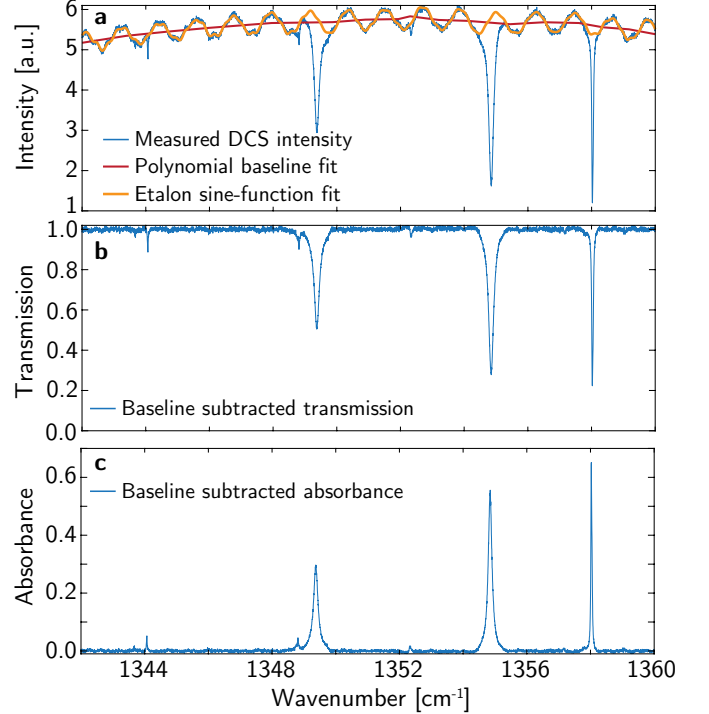

Fig. S2. Baseline correction procedure for atmospheric water absorption. (a) The measured transmitted spectra of the dual-comb system (blue curve) along with the fitted low-order polynomial baseline (red) and the fitted sine-function (orange) to correct for the mid-IR etalons. (b) The baseline subtracted transmission spectra along with the (c) absorbance spectra of the atmospheric water. Presented data is measured with the waveguide width of 2.95 µm and plotted as an example to clarify our baseline correction procedure for all other frequency ranges reported in the manuscript.

frame of reference of the pump pulse, ω_0 is the pump angular frequency, A_{eff} is the effective area of the waveguide mode, α is the linear loss, γ is the waveguide nonlinearity and is given by $\gamma = \frac{n_2 \omega_0}{c A_{eff}}$ with c being the speed of light and n_2 the nonlinear index of Si at the pump wavelength, β_{3PA} is the three-photon absorption (3PA) coefficient, σ is the free-carrier absorption (FCA) cross-section, and μ is the free-carrier dispersion (FCD) cross-section. N_c is the free-carrier density in the waveguide which evolve as:

$$\frac{\partial N_c(z,t)}{\partial \tau} = -\frac{N_c}{\tau_{eff}} + \frac{\beta_{3PA}}{3\hbar\omega_0 A_{eff}^3}|E(z,t)|^6$$

(S2)

where τ_{eff} is the free carrier relaxation time.

We solve the gNLSE using the split-step Fourier method (SSFM) with an adaptive step-size algorithm using the following parameters: $\alpha = 2$ dB/cm, $n_2 \approx 2.5 \times 10^{-5}$ cm^2/GW [4], $\omega_0 \approx 2\pi \times 98$ THz, $\beta_{3PA} = 1.75 \times 10^{-3}$ cm^3/GW^2 [4], and $\sigma = 5.65 \times 10^{-17}$ cm^2 [2]. The FCD cross-section, μ, depends on the free-carrier absorption cross-section (σ), coupled peak power, pulse duration, 3PA coefficient, pump frequency, and effective area of the waveguide mode with the mathematical equation derived in Ref. [5]. The effective area of the mode, $A_{eff} \approx 2$ µm^2, is calculated via finite-element-method analysis for each waveguide width individually. The free-carrier relaxation time is set to
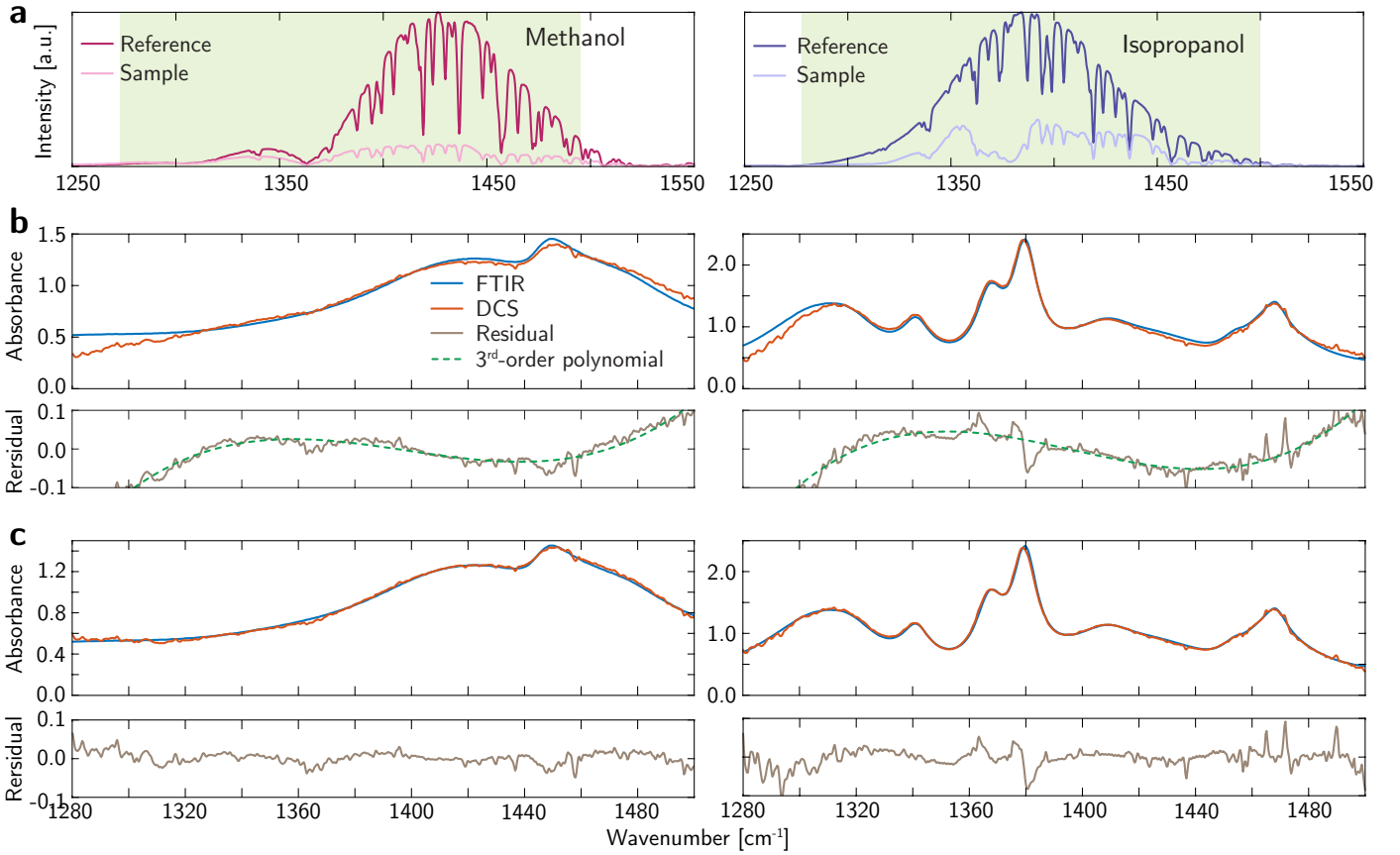
Fig. S3. Broadband baseline correction procedure for methanol and isopropanol dual-comb data. (a) The simultaneously measured reference and sample spectra for methanol and isopropanol on left and right columns, respectively. (b) The DCS measured absorbance spectra of isopropanol and methanol compared with FTIR measurements. The sample data is normalized to the reference for baseline subtraction. The experimental residuals are calculated as DCS data minus FTIR and presented in the bottom panels along with the 3rd-order polynomial fits to the residuals. The polynomial fits to both methanol and isopropanol residuals result in very similar polynomial curves. This similarity is a signature of a systematic different between our dual-comb system and the commercial FTIR used as the reference. (c) Comparison between DCS data and FTIR after removing the fitted 3rd-order polynomial function from the DCS data. The new residuals are calculated as residuals in (b) minus the polynomial fit. The polynomial fitting acts as a second degree baseline correction mechanism.

$\tau_{eff} = 1\ ns$ [6]. The coupled-in pulse is measured to be Gaussian pulse centered at $\lambda = 3.06$ µm with a full-width half-maximum (FWHM) duration of 85 fs and coupled peak power of 1.18 kW.

3. ATMOSPHERIC WATER ABSORPTION

To calculate the absorbance of the atmospheric water, we first need to remove the spectral baseline and mid-IR etalons from the measured dual-comb transmitted spectrum (Fig. S2a). We estimate the spectral baseline using a low-order polynomial fit (red curve in Fig. S2a) with added sine-function terms to account for the mid-IR etalons (orange curve in Fig. S2a). We then calculate the transmission spectrum of the dual-comb system (Fig. S2b) as I/I_0, where I_0 and I are the calculated baseline and the measured transmitted intensity spectrum, respectively. As the last step the absorbance (Fig. S2c) is defined according to the Beer-Lambert law as $A = \log_{10}(I/I_0)$.

For comparison to HITRAN, we use the water absorption cross-sections and line intensities from the database in a Voigt fitting algorithm. This algorithm accounts for temperature dependent Doppler shift of the center frequencies, Doppler broadening with Gaussian line shape, and Lorentzian line shape pressure

dependent broadening. We estimate the atmospheric pressure and water concentration by fitting the Voigt line shapes and intensities to the DCS data. In doing so, we keep the experimental temperature constant at 296 K while beam path length, experimental atmospheric pressure and volume-mixing ratio of water content are fitted into the algorithm to minimize the residuals between DCS data and HITRAN prediction. The fitting is performed on multiple spectral peaks within all frequency ranges accessed by the three waveguide widths of 3.35 µm, 2.95 µm, and 2.80 µm. We then report the mean value of all fitted atmospheric pressures and volume-mixing ratios of the water content as the environmental parameters of the experiment with the RMS difference between individual values and the calculated mean as the error bar of the estimated values.

4. BROADBAND BASELINE CORRECTION

The dual-comb measured sample and reference spectra are presented in Fig. S3a for methanol and isopropanol on left and right columns, respectively. To calculate the absorbance from the Beer-Lambert law, we initially remove the spectral baseline by dividing the sample spectra to their respective reference

measurement. We compare the results with identical measurements performed using a commercial Fourier transform infrared spectrometer (FTIR) in Fig. S3b. The dual-comb spectroscopy (DCS) data agrees well with the FTIR, however, the residuals for both chemicals show a very similar 3rd-order polynomial pattern. This pattern is studied further by fitting individual polynomial curves to both residuals. We realize that the same polynomial curve fits to both data. The fitted function is defined as $R(f) = a_3 f^3 + a_2 f^2 + a_1 f + a_0$, where R is the fitted polynomial function and f is the frequency. $a_3 = 2.49 \times 10^{-7}$, $a_2 = -0.001$, $a_1 = 1.46$, and $a_0 = -678$ are the fitted 3rd-order polynomial coefficients.

The fact that the same 3rd-order polynomial function explains the residual baselines of two independent measurements, points to a systematic difference between our dual-comb system and the commercial FTIR used in this experiment. We account for the observed different between DCS and FTIR measurements by removing the fitted polynomial function from the DCS data. Results of this step are presented in Fig. S3c. There is an excellent agreement between the DCS and FTIR data after the 3rd-order polynomial baseline correction with spectral residuals limited to the uncorrected atmospheric water absorption in this spectral region.

5. ABSORBANCE PEAK ASSIGNMENTS

We identify the measured absorbance peaks of methanol and isopropanol as various C—H and O—H bending vibrations. The most compelling infrared signature is the absorbance peak doublet around 1360–1400 cm^{-1} in the isopropanol spectrum (Fig. S4). This is a characteristic of the presence of a geminal dimethyl group, two CH$_3$ groups attached to a central carbon atom carrying an OH group ([7, 8], insets of Fig. S3). This is corroborated by the weaker lower frequency band indicative of a secondary alcohol [8]. Such observation in this region can be used to non-destructively identify the presence of secondary and tertiary alcohols with specificity that the 2–3 μm spectral region does not offer [7].

For a more specific assignment of the measured peaks, we use the Gaussian 03 and GaussView computational chemistry softwares [9] to simulate the relative peak positions and integrated intensities of the different C—H and O—H bending vibrations in liquid phase methanol and isopropanol. For methanol, three spectral features are recorded, two spectral peaks at 1422 cm^{-1} and 1450 cm^{-1} with a spectral shoulder at 1476 cm^{-1}. Reference [10] identifies these as $\nu'_6{}^{CH_3}$, $\nu''_6{}^{CH_3}$, and $\nu_3{}^{CH_3}$ bending vibrations, respectively. We assign the 1420 cm^{-1} peak to CH$_3$ bending with an umbrella-like wagging motion of hydrogen atoms. The 1450 cm^{-1} peak is assigned as the CH$_3$ bending with a scissoring motion in all three hydrogen atoms. The spectral shoulder at 1476 cm^{-1} is assigned to the CH$_3$ bending vibration with two of the hydrogen atoms undergoing scissoring motion.

For isopropanol, the following six absorbance peaks are measured (Fig. S4b): (1) O—H bending in symmetry-plane of the molecule at 1311 cm^{-1}, (2) wagging motion of the hydrogen atom in O—C—H group at 1341 cm^{-1}, (3) O—C—H group hydrogen bending in symmetry-plane of the molecule at 1368 cm^{-1}, (4) asymmetrical wagging motion in the CH$_3$ group at 1379 cm^{-1}, (5) symmetrical umbrella like wagging motion in the CH$_3$ along with in-plane bending of the O—H group at 1409 cm^{-1}, and (6) scissoring motion in the CH$_3$ while the O—H group is stationary at 1468 cm^{-1}. It is worth noting that Gaussian 03 calculations and GaussView visualizations are of the
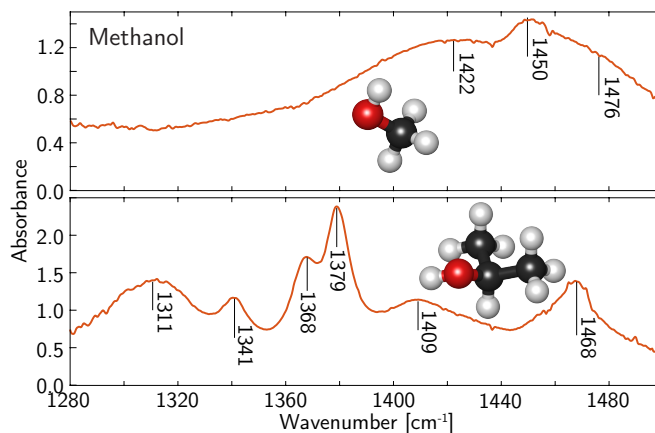

Fig. S4. The DCS absorbance spectra of methanol and isopropanol, with the frequency of the measured O—H and C—H bending vibration lines marked.

isolated molecule's eigenfrequencies and eigenmodes. The measured frequencies in the condensed phase samples are shifted due to interactions in the liquid. Assignments were made based on the eigenfrequencies and reported motions from GaussView [9] and Herzberg [10].

REFERENCES

1. J. Chiles, S. Khan, J. Ma, and S. Fathpour, "High-contrast, all-silicon waveguiding platform for ultra-broadband mid-infrared photonics," Appl. Phys. Lett. **103**, 151106 (2013).
2. Q. Lin, O. J. Painter, and G. P. Agrawal, "Nonlinear optical phenomena in silicon waveguides: Modeling and applications," Opt. Express **15**, 16604–16644 (2007).
3. R. K. W. Lau, M. R. E. Lamont, A. G. Griffith, Y. Okawachi, M. Lipson, and A. L. Gaeta, "Octave-spanning mid-infrared supercontinuum generation in silicon nanowaveguides," Opt. Lett. **39**, 4518–4521 (2014).
4. X. Gai, Y. Yu, B. Kuyken, P. Ma, S. J. Madden, J. Van Campenhout, P. Verheyen, G. Roelkens, R. Baets, and B. Luther-Davies, "Nonlinear absorption and refraction in crystalline silicon in the mid-infrared," Laser & Photonics Rev. **7**, 1054–1064 (2013).
5. N. Nader, D. L. Maser, F. C. Cruz, A. Kowligy, H. Timmers, J. Chiles, C. Fredrick, D. A. Westly, S. W. Nam, R. P. Mirin, J. M. Shainline, and S. Diddams, "Versatile silicon-waveguide supercontinuum for coherent mid-infrared spectroscopy," APL Photonics **3**, 036102 (2018).
6. B. Kuyken, T. Ideguchi, S. Holzner, M. Yan, T. W. Hansch, J. Van Campenhout, P. Verheyen, S. Coen, F. Leo, R. Baets, G. Roelkens, and N. Picqué, "An octave-spanning mid-infrared frequency comb generated in a silicon nanophotonic wire waveguide," Nat. Comm. **6**, 6310 (2015).
7. D. R. Klein, *Organic chemistry* (John Wiley, Hoboken, NJ, 2012).
8. R. W. Hannah and J. S. Swinehart, *Experiments in techniques of infrared spectroscopy* (Perkin-Elmer, Norwalk, CT, 1974).
9. M. J. Frisch, G. W. Trucks, H. B. Schlegel, G. E. Scuseria, M. A. Robb, J. R. Cheeseman, J. A. Montgomery, Jr., T. Vreven, K. N. Kudin, J. C. Burant, J. M. Millam, S. S. Iyengar, J. Tomasi, V. Barone, B. Mennucci, M. Cossi, G. Scalmani, N. Rega, G. A. Petersson, H. Nakatsuji, M. Hada, M. Ehara, K. Toyota, R. Fukuda, J. Hasegawa, M. Ishida,

T. Nakajima, Y. Honda, O. Kitao, H. Nakai, M. Klene, X. Li, J. E. Knox, H. P. Hratchian, J. B. Cross, V. Bakken, C. Adamo, J. Jaramillo, R. Gomperts, R. E. Stratmann, O. Yazyev, A. J. Austin, R. Cammi, C. Pomelli, J. W. Ochterski, P. Y. Ayala, K. Morokuma, G. A. Voth, P. Salvador, J. J. Dannenberg, V. G. Zakrzewski, S. Dapprich, A. D. Daniels, M. C. Strain, O. Farkas, D. K. Malick, A. D. Rabuck, K. Raghavachari, J. B. Foresman, J. V. Ortiz, Q. Cui, A. G. Baboul, S. Clifford, J. Cioslowski, B. B. Stefanov, G. Liu, A. Liashenko, P. Piskorz, I. Komaromi, R. L. Martin, D. J. Fox, T. Keith, M. A. Al-Laham, C. Y. Peng, A. Nanayakkara, M. Challacombe, P. M. W. Gill, B. Johnson, W. Chen, M. W. Wong, C. Gonzalez, and J. A. Pople, "Gaussian 03, Revision B.05," Gaussian, Inc., Pittsburgh PA, 2003.

10. G. Herzberg, *Molecular Spectra and Molecular Structure: II. Infrared and Raman Spectra of Polyatomic Molecules* (D. Van Nostrand Company, Inc., Princeton, NJ, 1992), tenth ed.